

Self-similarity, density-size dynamics and the sinking speed of marine aggregates

Andre Visser¹ and Anton Vergod Almgren¹

¹National Institute of Aquatic Resources, Technical University of Denmark

November 24, 2022

Abstract

* Poor estimates of the sinking speed of marine aggregates stem primarily high variance in aggregate excess density. * Self-similarity of aggregation facilitates efficiently modelling of aggregate size and excess density, and hence sinking speed. * This provides a mechanistic description of how planktonic communities impact the size and density-resolved export flux of organic matter.

1 **Self-similarity, density-size dynamics and the sinking**
2 **speed of marine aggregates.**

3 **Andre W. Visser¹, Anton Vergod Almgren¹**

4 ¹VKR Centre for Ocean Life, National Institute of Aquatic Resources, Technical University of Denmark,
5 Kongens Lyngby, Denmark

6 **Key Points:**

- 7 • Poor estimates of the sinking speed of marine aggregates stem primarily high vari-
8 ance in aggregate excess density.
9 • Self-similarity of aggregation facilitates efficiently modelling of aggregate size and
10 excess density, and hence sinking speed.
11 • This provides a mechanistic description of how planktonic communities impact
12 the size and density-resolved export flux of organic matter.

Corresponding author: A.W. Visser, awv@aqu.dtu.dk

Abstract

We propose self-similarity of aggregation provides a tractable framework for estimating the sinking speed of natural marine particle aggregates for ocean biogeochemical models. It does so by providing a means to tracking both size and excess density of aggregates as they are formed and transformed by aggregation, degradation and fragmentation processes. A self-similarity parameter a in the range 1.8 to 2.1 is well supported by direct observations drawn from an extensive database of aggregate size and sinking speed. This provides a mechanistic description of how spatial and temporal variations in planktonic communities impact size and density characteristic of aggregate assemblages and their subsequent export from the surface ocean. We provide a simple model for which we conduct sensitivity analyses for the self-similarity parameter, stickiness, and turbulent dissipation rate. While incomplete in several aspects, the model compares well with observations of aggregate size spectra covering the global ocean.

Plain Language Summary

How fast dead stuff sinks is perhaps the biggest uncertainty in estimating how the world's oceans cycle elements, and in particular, how they sequester carbon. We present a model that links surface plankton communities with the density and size characteristics of the aggregates of dead material they produce, and are thus able to estimate the sinking speeds of all aggregates that emerge. A key assumption that allows for efficient simulation is self-similarity of aggregation; that the underlying process of how aggregates form is well described by a set of global rules, even though this is often hidden by differences in what they are made of, and how they are degraded and fragmented. Although really quite simple, our model compares well with macroscopic properties of aggregate assemblages seen in nature.

1 Introduction

Perhaps the greatest hurdle to attaining a mechanistic understanding of the oceans' biogeochemical cycles is the incomplete description of the sinking speeds of particulate matter. This issue is central to key questions such as how much organic material is exported from the sunlit surface ocean (Ducklow et al., 2001; Mouw et al., 2016), its dependence on the ever changing structure of the surface plankton community (Boyd & Newton, 1995; Henson et al., 2012), the depth to which detrital material sinks before being solubilized (Cavan et al., 2017; Marsay et al., 2015), what this means for carbon sequestration (Kwon et al., 2009), consumption of oxygen (Suess, 1980; Bopp et al., 2002) nutrient recycling (Tréguer & Jacques, 1992; Buesseler et al., 2007), and how much reaches the seabed to be buried in sediments or feed benthic communities (Gooday, 2002; Cael, Bisson, et al., 2021). Despite years of observations from laboratory and field, sinking speeds of natural aggregate particles remain as enigmatic as ever; aggregates of any size from microns to centimeters seemingly sink at any speeds from practically zero to several 1000s of meters per day (Iversen & Lampitt, 2020; Laurenceau-Cornec et al., 2020; Cael, Cavan, & Britten, 2021). Yet the physics of sinking speed is unequivocal. Sinking speed is set by a balance between buoyancy forces and drag (Stokes, 1851; Clift et al., 1978), and while the precise formulation may not be as neat as Stokes' law (Oseen, 1910; White, 1991; Loth, 2008), the following principle must hold: sinking speed is a monotonically increasing function of aggregate size and excess density *ceteris paribus*.

The key concept we explore here is that aggregation is a geometrically self-similar process, such that the linear dimension r_{ioj} of an aggregate formed by the combination of two parent aggregates of linear dimension r_i and r_j respectively is given by:

$$r_{ioj} = (r_i^a + r_j^a)^{1/a} \quad (1)$$

60 That is, for the binary process of aggregation, r^a is an additive conservative property.
 61 This is not a new idea (Jackson, 1998; Wiesner, 1992) and arises from the general ob-
 62 servation that aggregates are fractal objects (Alldredge & Gotschalk, 1988; Meakin, 1987;
 63 Logan & Wilkinson, 1990). We term a the self-similarity parameter, and note $a < 3$
 64 in compliance with the observed increase in porosity under aggregation. We stress that
 65 a is not the fractal dimension of the aggregate. Neither is it an inherent property of ag-
 66 gregates and we will not attempt to use a to produce scaling laws as is the usual trajec-
 67 tory of these considerations. At this point we simply want to treat a as a parameter gov-
 68 erning the binary process of aggregation.

69 Under geometric self-similarity, the total mass of an aggregate produced by the com-
 70 bination of 2 aggregates of mass m_i and m_j can be deduced to be the sum of these two
 71 masses, plus a bit extra due to the inclusion of some fluid (density ρ_w) that occupies the
 72 expanded aggregate volume (i.e. increase in porosity). Specifically,

$$m_{ioj} = m_i + m_j + (v_{ioj} - v_i - v_j)\rho_w \quad (2)$$

73 where v_i , v_j and v_{ioj} are the volumes of the two parent aggregates and the daughter ag-
 74 gregate respectively. Note that m is the total mass, not just the dry mass of the aggre-
 75 gate. It is convenient to recast this in terms of density of the aggregates, ρ_i , ρ_j , ρ_{ioj} . It
 76 follows that excess density

$$\rho_{ioj} - \rho_w = \frac{r_i^3}{r_{ioj}^3}(\rho_i - \rho_w) + \frac{r_j^3}{r_{ioj}^3}(\rho_j - \rho_w) \quad (3)$$

77 Equations (1) and (3) provide a construct by which the size and excess density, and
 78 hence sinking speed, of particle aggregates can be estimated. However, processes other
 79 than aggregation also effect size and density; chief amongst these are degradation, dis-
 80 solution and fragmentation. This is illustrated in Figure 1 for a single primary particle
 81 (a diatom for instance) where aggregation produces larger and less dense aggregates, degra-
 82 dation and /or dissolution removes mass but has no immediate impact on aggregate size,
 83 and fragmentation, particularly on large porous aggregates produces smaller aggregates
 84 which can be reincorporated into the aggregation process. Though out, sinking speed
 85 can be estimated. At the system scale (*e.g.* the surface mixed layer), a dynamic can be
 86 established between the supply of primary particles (*e.g.* from primary production, de-
 87 position of dust, faecal pellets) and the loss of aggregates by sinking. While still rela-
 88 tively complex, each of the sub-processes can in principle be constrained from observa-
 89 tions, parameterized and mechanistically formulated. What makes this framework par-
 90 ticularly attractive is the development of size-based and trait-based models of plankton
 91 communities (Banas, 2011; Serra-Pompei et al., 2020; Serra-Pompei et al., 2022) which
 92 provide precisely the type of information (size and trait resolved primary productivity
 93 and zooplankton grazers) that can serve as input. Indeed a resolved particle aggrega-
 94 tion model can provide a mechanistic link between emerging plankton community struc-
 95 ture and export flux; one of the key unresolved issues of the biological carbon pump (Boyd
 96 & Newton, 1995; Bach et al., 2019).

97 **2 Analysis of self-similarity from observations.**

98 A large literature exists reporting observations of the sinking speed and size of ma-
 99 rine aggregates. These were recently collated and published in a database (Laurenceau-
 100 Cornec et al., 2015; Cael, Cavan, & Britten, 2021), and, together with additional obser-
 101 vations (Gärdes et al., 2011; Bach et al., 2019; Iversen & Lampitt, 2020) provide the ba-
 102 sis for this analysis. While aggregate density in itself is a difficult parameter to measure,
 103 it can be estimated from observed sinking speeds (Engel et al., 2009; Iversen & Ploug,
 104 2010). In particular,

$$\rho - \rho_w = \frac{3}{8} \frac{Cw^2}{gr} \quad (4)$$

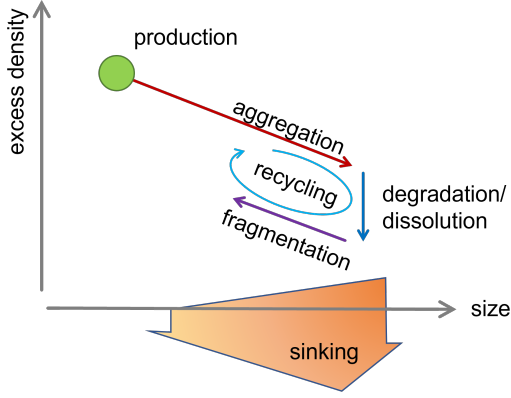


Figure 1. Aggregate dynamics depicted in 2 dimensional state space. Dynamics are driven by 3 processes; aggregation producing larger less dense aggregates, degradation/dissolution which reduces the solid mass (and hence excess density) of aggregates, and fragmentation. Primary particles (e.g. diatoms) are produce in a specific size and density range. The production of other material such as dust and TEP can also be specified. The distribution of aggregates in this state space eventually reaches steady state when the rate of supply is balanced by the sinking losses particularly of large dense aggregates.

106 where w is sinking speed, r the estimated spherical radius, g the gravitational acceler-
 107 ation, and C is an empirically derived drag coefficient. While there are several formul-
 108 ations, generally expressed as a function of Reynolds number ($R = 2rw/\eta$, with η be-
 109 ing the kinematic viscosity of seawater), the most commonly used is

$$110 \quad C = \frac{24}{R} + \frac{6}{1 + \sqrt{R}} + 0.4 \quad (5)$$

111 (White, 1991). This, and similar formulas are robust for R up to about 10^5 . Estimates
 112 of excess density and observed sinking speed for aggregates are plotted in Figure 2 and
 113 summarized in Table 1. The preponderance of observations correspond to $R < 100$ and
 114 thus lie well within the range where (5) is valid. The general features of Figure 2 neatly
 115 illustrate some of the properties of aggregation already mentioned. For instance, that
 116 large aggregates tend to sink faster and have a lower excess density than small aggre-
 117 gates. Further, while there is considerable variance of sinking speed with size, this ap-
 118 pears to be reduced for excess density. Indeed, the ensemble of excess density observa-
 119 tions appears to collapse roughly to a power law r^b with b around -1.4 .

120 Under special conditions, self-similarity makes quite strong predictions on how ag-
 121 gregate properties (e.g. mass, density, porosity) scale with size. Specifically, for a mono-
 122 culture of primary particles of size r_0 and density ρ_0 , and in the absence of degradation,
 123 dissolution, and fragmentation, then aggregates' excess density follows a power law:

$$\rho(r) - \rho_w = (\rho_o - \rho_w) \left(\frac{r}{r_0} \right)^{a-3} \quad (6)$$

124 Under these conditions, the aggregation vector in the Figure 1, would have an expected
 125 slope $a - 3$.

126 Within the set of field and laboratory observations reported in Table 1, a subset
 127 meet suitable criteria that can reveal such a relationship. For instance, (Iversen & Ploug,
 128 2010) conducted laboratory studies of aggregates from relatively fresh monocultures of
 129 the chain forming diatom *Skeletonema costatum* and the coccolithophore *Emiliania hux-*
 130 *leyi*, and mixtures of the two. Log-log regressions on these indicate b in the range -1.2

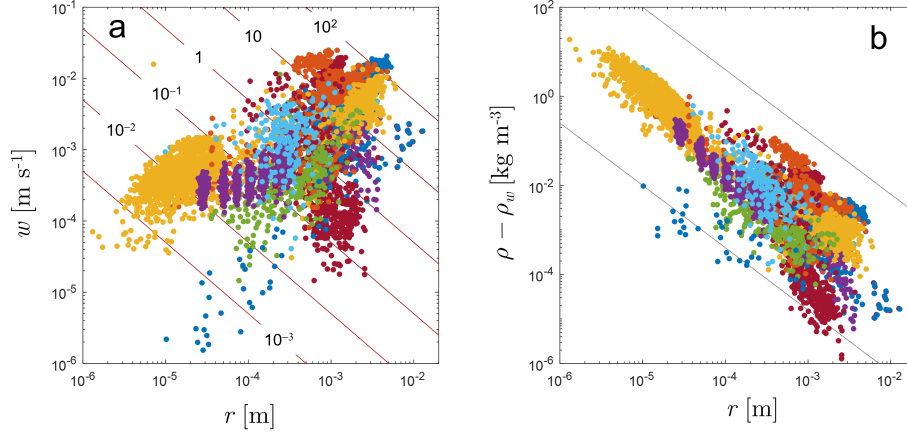


Figure 2. (a) Aggregate sinking speed (w) observed in a large number of studies (cf. Table 1) as a function of estimated spherical radius (r) and (b) the excess density ($\rho - \rho_w$) calculated from observed sinking speeds using a modified Stokes law. Colors represent different studies. The lines in panel (a) are contours of Reynolds number ranging from 100 to 0.001. The grey lines in panel (b) indicate a log-log slope of -1.4 .

131 to -1.0 i.e. a in the range 1.8 to 2.0. Other laboratory observations that have avoided
 132 degradation and extraneous manipulations with TEP and dust indicate similar relation-
 133 ships with b in the range $[-1.2, -0.9]$ (Engel & Schartau, 1999; Engel et al., 2009; Laurenceau-
 134 Cornec et al., 2015). These values are consistent with laboratory experiments for non-
 135 biological particle aggregation (Lin et al., 1989) for which a ranges between 1.8 and 2.1.
 136 The lower value corresponds to a relatively porous structure that arises when aggregates
 137 are built-up of very sticky, similarly sized particles that combine immediately on con-
 138 tact. The value $a = 2$ corresponds to a random walk arrangement in 3 dimensions, and
 139 has been used in previous model settings (Jackson & Burd, 1998; Jokulsdottir & Archer,
 140 2016). From these considerations, it appears that a in the ranges 1.8 to 2.1 is a reason-
 141 able choice.

142 It is also clear that a large number, indeed the majority, of studies listed in Table
 143 1, exhibit slopes b that are spread across a much broader range. These studies all fol-
 144 low quite different experimental (e.g. natural aggregates, lab cultures, manipulations with
 145 ballast material) and observational procedures (e.g. *in situ* cameras, roller tanks, ver-
 146 tical flow systems). In some instances it can be argued that the observation method is
 147 poorly designed to capture the characteristics of the full aggregate community. Roller
 148 tanks for instance preferentially generate large, fast-sinking aggregates (Jackson, 2015)
 149 producing particle size spectra that are not representative of natural aggregate commu-
 150 nities. Perhaps more important is the heterogeneity of the primary particles. In some
 151 experimental setups, ballasting material of considerably different excess densities are present
 152 or introduced. Further, natural plankton communities are seldom mono-cultures, and
 153 are generally composed of unicellular organisms covering a range of sizes and densities;
 154 some with shells and spines, some vacuolated, some chain-forming. In any given size range,
 155 the aggregate community will be an ad-mixture derived from different primary particles.
 156 Furthermore, as aggregates degrade and fragment, smaller, less dense aggregates come
 157 into the mix – grist to the mill – so that aggregate density, and hence sinking speed, will
 158 exhibit a relatively broad distribution at any given aggregate size. We must therefore
 159 conclude that while the majority of observations plotted in Figure 2 are perfectly fine
 160 in relating the sinking speed to the size of an aggregate, methodological issues mean that

161 they remain mute on any self-similarity in the underlying aggregation process. Seen in
 162 this light, it appears that the variance of excess density (Figure 2 (b)) is composed of
 163 two elements; a general negative slope being due to increased aggregate porosity with
 164 size, and an inherent variability due to the excess density of primary aggregate mate-
 165 rial.

166 3 Dynamic Aggregate Model

167 Here we provide a brief description of a simplified model . The physical setting we
 168 consider is a surface mixed layer of depth h where aggregates are produced from a range
 169 of primary particles, transformed and sink out according to the dynamics described in
 170 Figure 1. The model simulates the number and mass of aggregates in a two dimensional
 171 state space (size and excess density). We supply the code for the model in the supple-
 172 mentary material, and encourage readers to perform their own simulations.

173 It is convenient right from the outset to introduce two transformed variable (x, z)
 174 that map to $(r, \rho - \rho_w)$ as

$$175 \quad r = r_o \delta^x, \quad \rho - \rho_w = \rho_o z \delta^{(a-3)x} \quad (7)$$

176 x is a logarithmic scaling of aggregate size, and z a stretched linear scaling of excess den-
 177 sity. The factor $\delta^{(a-3)x}$ takes advantage of the reduction of density by aggregation and
 178 expands the density resolution for large aggregates. Key variables in the model are the
 179 matrices \mathbf{N} and \mathbf{M} representing the number of aggregates and their total mass respec-
 180 tively within 1×1 bins in discretized (x, z) state space. Suitable range choices for x and
 181 z , scaling factors r_o [μm] and ρ_o [kg m^{-3}], and logarithmic interval δ allow for a rela-
 182 tively complete representation of the aggregate community within computationally con-
 183 venient dimensions of \mathbf{N} and \mathbf{M} . These are related by $\mathbf{M} = \mathbf{m} \circ \mathbf{N}$ where \circ represents
 184 piece-wise matrix product and \mathbf{m} is the mean mass of an aggregate within each bin.

185 The model determines the rate of change of \mathbf{M} due to five processes: production,
 186 aggregation, degradation, fragmentation and sinking losses. Several of these processes
 187 are relatively simple to implement. For instance production is prescribed and sinking losses
 188 $\mathbf{Q} = -\mathbf{M}\mathbf{ow}/h$, where w is the mean aggregate sinking speed in discretized state space.
 189 Aggregation is computationally the most complex aspect of the model as it involves a
 190 binary convolution of \mathbf{N} (Smoluchowski, 1916). It is governed by encounter kernels β ;
 191 the rate at which aggregates collide, and stickiness α ; the probability that collision will
 192 lead to aggregation (Burd & Jackson, 2009; Jokulsdottir & Archer, 2016). Performing
 193 binary convolution calculations is greatly facilitated by self-similarity. Specifically, the
 194 ordinates of an aggregate produced from the combination of (x_i, z_i) and (x_j, z_j) is given
 195 by:

$$\begin{aligned} x_{i \circ j} &= x_i + \log_{\delta}((1 + \delta^{(x_j - x_i)a})/a) \\ &= x_j + \log_{\delta}((1 + \delta^{(x_i - x_j)a})/a) \\ z_{i \circ j} &= \frac{z_i}{1 + \delta^{(x_j - x_i)a}} + \frac{z_j}{1 + \delta^{(x_i - x_j)a}}. \end{aligned} \quad (8)$$

196 It follows that the combination of aggregates from any two 1×1 bins in state space will
 197 be confined to a third 1×1 bin, albeit offset from the matrix grid spacing. The model
 198 utilizes this in optimizing the algorithm architecture.

199 We implement degradation as a drift of particle numbers to lower density bins. Specif-
 200 ically, if γ is the degradation rate, then it can be shown that the z ordinate of an aggre-
 201 gate follows $dz/dt = -\gamma z$. In this, degradation acts only on excess density. We set $\gamma =$
 202 0.1 day^{-1} consistent with a range of studies (Kjørboe, 2001; Cavan & Boyd, 2018; Bach
 203 et al., 2019) although it should be noted that there is considerable variation. Finally frag-
 204 mentation is simulated simply as a rate at which aggregate mass is transported to smaller

205 sizes classes. We implement this as an increasing function of aggregate size. Of the pro-
 206 cesses considered, fragmentation remains the least well constrained; aggregates appear
 207 resistant to mechanical shear (Alldredge et al., 1990), and fragmented appears to be chiefly
 208 mediated by metazoans through handling and feeding appears to be important (Dilling
 209 & Alldredge, 2000) and by microbial "mining" and dissolution of adhesive material. We
 210 set the maximum fragmentation rate at 0.5 day^{-1} for large porous aggregates, a value
 211 consistent with observations (Briggs et al., 2020).

212 4 Results and sensitivity

213 We present a series of simulations for a fixed rate of primary particle production
 214 (size range 1 to 30 μm in radius, excess density range 10 to 100 kg m^{-3}) that corresponds
 215 to a mixed community of unicellular auto- and heterotrophic plankton ranging from cyanobac-
 216 teria to diatoms. Simulations were run to quasi-steady state (i.e. relative differences be-
 217 tween successive daily estimates (normalized root-mean-square deviation) were $< 10^{-6}$)
 218 using a MATLAB ode solver. Three sets of parameters (self-similarity, stickiness and tur-
 219 bulent dissipation rate) were varied between runs and the emerging aggregate commu-
 220 nity was characterized by its size spectrum and size resolved export flux. All simulations
 221 assumed a mixed layer depth of $h = 50 \text{ m}$, and a production rate of $P_{\text{total}} = 0.1 \text{ gC m}^{-2}$
 222 day^{-1} of primary detrital particles. Results are presented in Figure 3, and the numer-
 223 ical code that produced it can be found in the supplementary material.

224 Particle size spectra $n(r(x)) = \sum_z N(x, z)/dr(x)$ were estimated in the normal
 225 manner (Burd & Jackson, 2009) as per size bin width and provide a macroscopic mea-
 226 sure of the underlying dynamics of production, transformation and sinking. Measure-
 227 ments of such spectra are routinely made and often conform to a power law of the form
 228 $n(r) \sim r^p$. Observations (Stemmann et al., 2008; Guidi et al., 2009; Reynolds & Stram-
 229 ski, 2021) from different oceanic regions and spanning aggregate sizes from microns to
 230 centimeters, show that p ranges from -2 to -6 and cluster around -3 to -4 in the sur-
 231 face ocean. For our model simulations (Figure 3:b,d,f), all runs exhibited particle size
 232 spectra slopes of about -4 for aggregates from 1 to several 100s of μm in size.

233 The flux distributions $f(r(x)) = \sum_z M(x, z) \circ w(x, z)/(hP_{\text{total}})$ are the flux con-
 234 tributions summed over different excess density bins, reported within aggregate size bins
 235 and normalized with regards total primary particle production P_{total} . The net sum is
 236 a little less than unity; difference being due to the net loss of mass due to degradation.
 237 The shape of $f(r)$ is universally dome-shaped with very little flux at either small (low
 238 sinking speed) or large (low total mass) aggregate sizes. The peak of the flux distribu-
 239 tion, and to some extent its width, varies with self-similarity, stickiness and turbulent
 240 dissipation rate. Low self-similarity indices for instance, push the flux distribution to-
 241 wards larger aggregate sizes, as do high turbulent dissipation rates. Stickiness by con-
 242 trast has a relatively minor influence on the flux distribution. Maximum flux appears
 243 to be associated with a steepening of the particle size spectrum $n(r)$.

244 While we have argued that a universal self-similarity index, if it exists, is relatively
 245 well constrained within the range $[1.8, 2.1]$, this range still presents a large variation in
 246 the characteristics of the export flux. For instance, the peak of the flux distribution (Fig-
 247 ure 3 a) ranges over an order of magnitude in aggregate size, from 300 to 3000 μm . Fur-
 248 ther, the flux distribution range is much narrower for high self-similarity indices, a fea-
 249 ture that is exacerbated given the logarithmic scaling of the size bins. The total export
 250 flux however, remains virtually the same across all these self similarity values (within
 251 99% of each other). Indeed, the self similarity parameter has counteracting effects on sink-
 252 ing speed in terms of aggregate size and excess density (large a produce small but low
 253 porous aggregates and vice versa). The sinking speeds for aggregates in flux maxima (Fig-
 254 ure 3 a) vary only modestly, from 10 to 20 m day^{-1} across all values of the self-similarity
 255 parameter. It should be noted that the export flux distribution in terms of aggregate size,

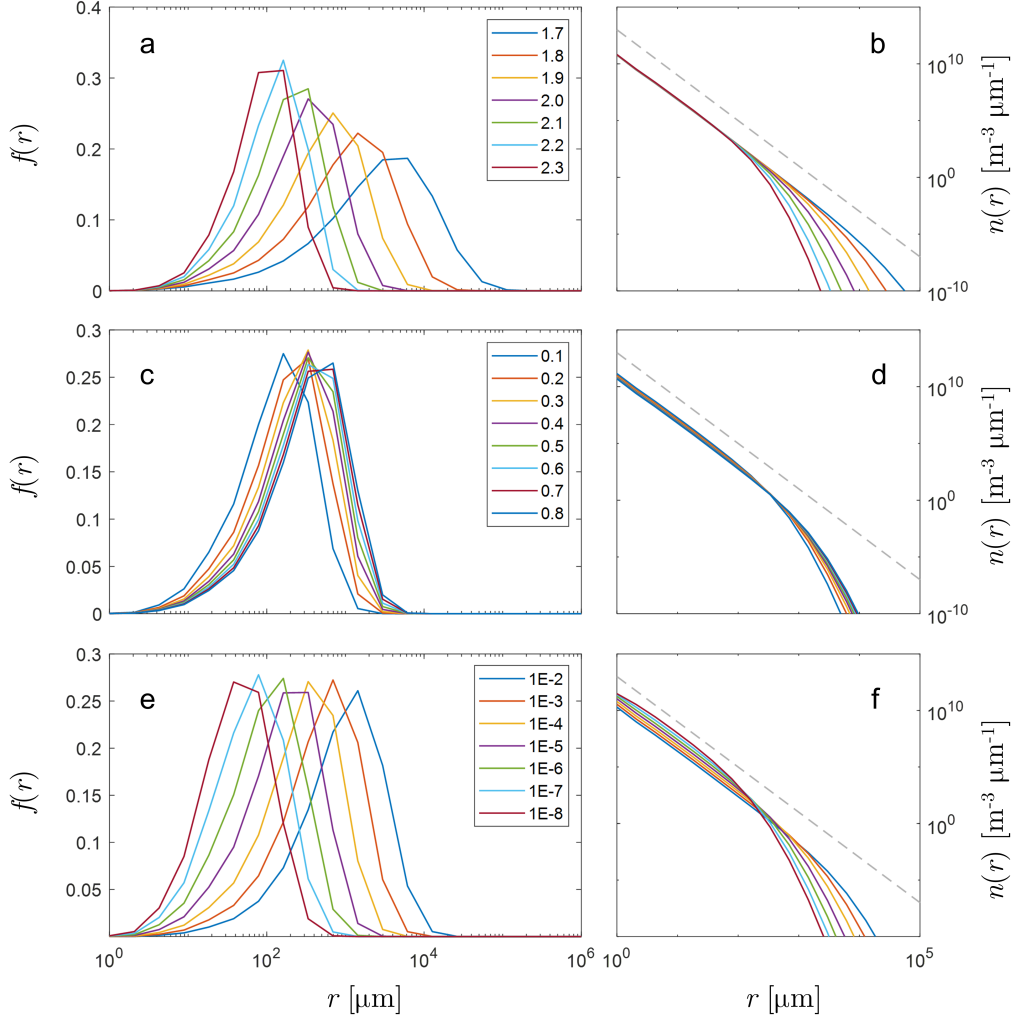


Figure 3. Aggregate community structure at steady state; $f(r)$ size resolved normalized export flux (a,c,b) and $n(r)$ particle size spectra (b,d,f) for a range of different a self-similarity parameters (a,b), α stickiness coefficients (c,d) and turbulent dissipation rates $[\text{m}^2 \text{s}^{-3}]$ (e,f). Dissipation rates are related to encounter rate β as given in (Burd & Jackson, 2009). Dashed lines in (b,d,f) indicate log-log slopes of -4 .

256 excess density and sinking speed sets many of the key characteristics of the subsequent
 257 flux attenuation curve within the mesopelagic (e.g. remineralization length scale (Cavan
 258 et al., 2017) and subsequent sequestration time scales (Boyd et al., 2019)). While we can-
 259 not at this time provide argumentation to further constrain the self-similarity param-
 260 eter, we have put in place a mechanistic model that can guide empirical studies to im-
 261 prove resolution.

262 5 Conclusions

263 Much of the literature concerning the fractal dimensions of aggregates has been built
 264 on the restrictive assumptions of irreversibility and uniform primary particles (Meakin,
 265 1987; Lin et al., 1989) which leads to the rather handy definition that the fractal dimen-
 266 sion of aggregates a' can be found from their mass-size relationship $m \sim r^{a'}$ (Meakin,
 267 1987; Burd & Jackson, 2009). At the same time, aggregates found in the marine envi-
 268 ronment have been deemed to be fractal objects in that they display fractal type prop-
 269 erties (Alldredge & Gotschalk, 1989; Logan & Wilkinson, 1990); an increase in poros-
 270 ity and a decrease in excess density as a function of size for instance. There is however
 271 a disconnect between these two concepts, namely that aggregation in the marine envi-
 272 ronment is not irreversible; aggregates degrade and fragment, and they are not composed
 273 of identical primary particles. All manner of primary particles are introduced into the
 274 surface ocean by primary producers, sloppy feeding, fecal matter and aeolian dust de-
 275 posits. Further, the constituent components of detritus vary significantly in excess den-
 276 sity (relative to seawater $\rho_w = 1027 \text{ kg m}^{-3}$) ranging from positively buoyant e.g. TEP
 277 in the range -200 to -300 kg m^{-3} (Azetsu-Scott & Passow, 2004) and lipids around -100
 278 kg m^{-3} (Visser & Jónasdóttir, 1999) to near neutrally buoyant e.g. cytoplasm 3 to 70
 279 kg m^{-3} (Tappan & Loeblich Jr, 1973), to very much negatively buoyant, e.g. coccol-
 280 iths 1700 to 1900 kg m^{-3} (Toktamış et al., 2016), diatom frustules 1600 kg m^{-3} (Miklasz
 281 & Denny, 2010) and atmospheric dust (quartz, feldspar, calcite) approximately 1700 kg
 282 m^{-3} . It is no surprise that neither a well constrained fractal dimension nor a size depen-
 283 dent sinking speed for marine aggregates has been found.

284 More than anything, the poor ability to estimate the sinking speed of marine ag-
 285 gregates stems from the high variability of their excess density. Other factors, like shape,
 286 surface roughness and the through flow of interstitial fluid have been suggested, but at
 287 most, contribute a factor 2 to sinking speed corrections. This is negligible compared to
 288 the orders of magnitude variance (yet alone a potential change in sign) exhibited in the
 289 excess density. The modelling framework we propose is designed specifically to track both
 290 size and excess density throughout an emerging aggregate community. We purposefully
 291 present the model itself in its simplest form. In this we are mindful that overly complex
 292 models become increasingly inscrutable, and unattractive for integration into higher level
 293 computational products. There are clearly aspects that can be expanded. For instance
 294 resolving aggregate porosity would allow a distinction between dry mass and total mass
 295 and provide a more robust implementation of degradation and fragmentation processes.
 296 Stickiness is also a parameter that shows large variability in primary material (from TEP
 297 to dust). Further, temporal aspects such as annual cycles of productivity, turbulence and
 298 mixed layer depth are yet to be explored. Finally, our concept of self-similarity of ag-
 299 gregation, and a governing parameter a constrained to the range 1.8 to 2.1 is certainly
 300 open to scrutiny, particularly given its impact on the emerging flux-size distribution. That
 301 there is some systematic control on aggregate size and density is evident in figure 2.b.
 302 How this is manifest in particular setting is however highly variable. We argue that in
 303 part, this variability can be accounted for through the aggregation process for which we
 304 provide a mechanistic description. A large part of the variance remains however, and re-
 305 flects the vastly different excess densities of the primary material from which the aggre-
 306 gates derive. Failure to recognize the variability in the density of primary material and

307 how this propagates through an aggregate community confounds efforts to estimate fluxes
 308 and attenuation length scales of particulate matter in the oceans.

309 6 Open Research

310 The model code and associated documentation for the simulations presented here
 311 is open source, and freely available on GitHub github.com/AndyWVisser/Aggregation
 312 and zenodo.org/record/6731544#.Yra-0HZBxPY. Data sets used in the analysis are avail-
 313 able in the supplementary material and accessible at zenodo.org/record/6731670#.Yra9i3ZBxPY.

314 Acknowledgments

315 This work was supported by the Centre for Ocean Life, a Villum Kann Rasmussen Cen-
 316 tre of Excellence supported by the Villum Foundation, by the Gordon and Betty Moore
 317 Foundation (grant 5479), and has received funding from the European Union’s Horizon
 318 2020 research and innovation programme under grant agreement No 869383 (ECOTIP).

319 References

- 320 Alldredge, A. L., & Gotschalk, C. (1988). In situ settling behavior of marine snow.
 321 *Limnology and Oceanography*, *33*(3), 339–351. doi: 10.4319/lo.1988.33.3.0339
- 322 Alldredge, A. L., & Gotschalk, C. C. (1989). Direct observations of the mass flocculation of diatom blooms: characteristics, settling velocities and formation of diatom aggregates. *Deep Sea Research Part I: Topical Studies in Oceanography*, *36*, 159–171. doi: 10.1016/0198-0149(89)90131-3
- 324 Alldredge, A. L., Granata, T. C., Gotschalk, C. C., & Dickey, T. D. (1990). The physical strength of marine snow and its implications for particle disaggregation in the ocean. *Limnology and Oceanography*, *35*(7), 1415–1428.
- 326 Azetsu-Scott, K., & Johnson, B. D. (1992). Measuring physical characteristics of particles: A new method of simultaneous measurement for size, settling velocity and density of constituent matter. *Deep Sea Research Part A. Oceanographic Research Papers*, *39*(6), 1057–1066. doi: 10.1016/0198-0149(92)90039-v
- 329 Azetsu-Scott, K., & Passow, U. (2004). Ascending marine particles: Significance of transparent exopolymer particles (TEP) in the upper ocean. *Limnology and oceanography*, *49*(3), 741–748.
- 334 Bach, L. T., Stange, P., Taucher, J., Achterberg, E. P., Algueró-Muñoz, M., Horn, H., . . . Riebesell, U. (2019). The influence of plankton community structure on sinking velocity and remineralization rate of marine aggregates. *Global Biogeochemical Cycles*, *33*(8), 971–994. doi: 10.1029/2019gb006256
- 337 Banas, N. S. (2011). Adding complex trophic interactions to a size-spectral plankton model: Emergent diversity patterns and limits on predictability. *Ecological Modelling*, *222*(15), 2663–2675. doi: 10.1016/j.ecolmodel.2011.05.018
- 341 Belcher, A., Iversen, M., Giering, S., Riou, V., Henson, S. A., Berline, L., . . . Sanders, R. (2016). Depth-resolved particle-associated microbial respiration in the northeast Atlantic. *Biogeosciences*, *13*(17), 4927–4943. doi: 10.5194/bg-13-4927-2016
- 344 Bopp, L., Le Quééré, C., Heimann, M., Manning, A. C., & Monfray, P. (2002). Climate-induced oceanic oxygen fluxes: Implications for the contemporary carbon budget. *Global Biogeochemical Cycles*, *16*(2), 6–1. doi: 10.1029/2001gb001445
- 348 Boyd, P. W., Claustre, H., Levy, M., Siegel, D. A., & Weber, T. (2019). Multifaceted particle pumps drive carbon sequestration in the ocean. *Nature*, *568*(7752), 327. doi: 10.1038/s41586-019-1098-2
- 352 Boyd, P. W., & Newton, P. (1995). Evidence of the potential influence of planktonic

- community structure on the interannual variability of particulate organic carbon flux. *Deep Sea Research Part I: Oceanographic Research Papers*, 42(5), 619–639. doi: 10.1016/0967-0637(95)00017-Z
- Briggs, N., Dall’Olmo, G., & Claustre, H. (2020). Major role of particle fragmentation in regulating biological sequestration of CO₂ by the oceans. *Science*, 367(6479), 791–793.
- Buesseler, K. O., Lamborg, C. H., Boyd, P. W., Lam, P. J., Trull, T. W., Bidigare, R. R., ... Wilson, S. (2007). Revisiting carbon flux through the ocean’s twilight zone. *Science*, 316(5824), 567–70. doi: 10.1126/science.1137959
- Burd, A. B., & Jackson, G. A. (2009). Particle aggregation. *Annual Review of Marine Science*, 1, 65–90. doi: 10.1146/annurev.marine.010908.163904
- Cael, B. B., Bisson, K., Conte, M., Duret, M. T., Follett, C. L., Henson, S. A., ... Lampitt, R. S. (2021). Open ocean particle flux variability from surface to seafloor. *Geophysical Research Letters*, 48(9), e2021GL092895. doi: 10.1029/2021gl092895
- Cael, B. B., Cavan, E. L., & Britten, G. L. (2021). Reconciling the size-dependence of marine particle sinking speed. *Geophysical Research Letters*, 48(5), e2020GL091771. doi: 10.1029/2020gl091771
- Carder, K. L., Steward, R. G., & Betzer, P. R. (1982). In situ holographic measurements of the sizes and settling rates of oceanic particulates. *Journal of Geophysical Research: Oceans*, 87(C8), 5681–5685. doi: 10.1029/jc087ic08p05681
- Cavan, E. L., & Boyd, P. W. (2018). Effect of anthropogenic warming on microbial respiration and particulate organic carbon export rates in the sub-Antarctic Southern Ocean. *Aquatic Microbial Ecology*, 82(2), 111–127.
- Cavan, E. L., Trimmer, M., Shelley, F., & Sanders, R. (2017). Remineralization of particulate organic carbon in an ocean oxygen minimum zone. *Nature Communications*, 8(1), 1–9.
- Clift, R., Grace, J. R., & Webber, M. E. (1978). *Bubbles, Drops and Particles*. San Diego: Academic Press.
- Diercks, A.-R., & Asper, V. L. (1997). In situ settling speeds of marine snow aggregates below the mixed layer: Black Sea and Gulf of Mexico. *Deep Sea Research Part I: Oceanographic Research Papers*, 44(3), 385–398. doi: 10.1016/S0967-0637(96)00104-5
- Dilling, L., & Alldredge, A. L. (2000). Fragmentation of marine snow by swimming macrozooplankton: A new process impacting carbon cycling in the sea. *Deep Sea Research Part I: Oceanographic Research Papers*, 47(7), 1227–1245.
- Ducklow, H. W., Steinberg, D. K., & Buesseler, K. O. (2001). Upper Ocean Carbon Export and the Biological Pump. *Oceanography*, 14(4), 50–58. doi: 10.5670/oceanog.2001.06
- Engel, A., Abramson, L., Szlosek, J., Liu, Z., Stewart, G., Hirschberg, D., & Lee, C. (2009). Investigating the effect of ballasting by CaCO₃ in *Emiliania huxleyi*, II: Decomposition of particulate organic matter. *Deep Sea Research Part I: Topical Studies in Oceanography*, 56(18), 1408–1419. doi: 10.1016/j.dsr2.2008.11.028
- Engel, A., & Schartau, M. (1999). Influence of transparent exopolymer particles (TEP) on sinking velocity of *Nitzschia closterium* aggregates. *Marine Ecology Progress Series*, 182, 69–76. doi: 10.3354/meps182069
- Gibbs, R. J. (1985). Estuarine flocs: their size, settling velocity and density. *Journal of Geophysical Research: Oceans*, 90(C2), 3249–3251. doi: 10.1029/jc090ic02p03249
- Gooday, A. J. (2002). Biological responses to seasonally varying fluxes of organic matter to the ocean floor: a review. *Journal of Oceanography*, 58(2), 305–332. doi: 10.1023/A:1015865826379
- Guidi, L., Jackson, G. A., Stemann, L., Miquel, J. C., Picheral, M., & Gorsky, G. (2008). Relationship between particle size distribution and flux in the

- 411 mesopelagic zone. *Deep Sea Research Part I: Oceanographic Research Papers*,
 412 55(10), 1364–1374. doi: 10.1016/j.dsr.2008.05.014
- 413 Guidi, L., Stemmann, L., Jackson, G. A., Ibanez, F., Claustre, H., Legendre, L.,
 414 ... Gorsky, G. (2009). Effects of phytoplankton community on production,
 415 size, and export of large aggregates: A world-ocean analysis. *Limnology and*
 416 *Oceanography*, 54(6), 1951–1963.
- 417 Gärdes, A., Iversen, M. H., Grossart, H.-P., Passow, U., & Ullrich, M. S. (2011).
 418 Diatom-associated bacteria are required for aggregation of *Thalassiosira weiss-*
 419 *flogii*. *ISME Journal*, 5(3), 436–445. doi: 10.1038/ismej.2010.145
- 420 Henson, S., Lampitt, R., & Johns, D. (2012). Variability in phytoplankton commu-
 421 nity structure in response to the North Atlantic Oscillation and implications
 422 for organic carbon flux. *Limnology and Oceanography*, 57(6), 1591–1601. doi:
 423 10.4319/lo.2012.57.6.1591
- 424 Hill, P. S., Syvitski, J. P., Cowan, E. A., & Powell, R. D. (1998). In situ observa-
 425 tions of flocc settling velocities in Glacier Bay, Alaska. *Marine Geology*, 145(1-
 426 2), 85–94. doi: 10.1016/s0025-3227(97)00109-6
- 427 Iversen, M. H., & Lampitt, R. S. (2020). Size does not matter after all: No evidence
 428 for a size-sinking relationship for marine snow. *Progress in Oceanography*, 189,
 429 102445. doi: 10.1016/j.pocean.2020.102445
- 430 Iversen, M. H., Nowald, N., Ploug, H., Jackson, G. A., & Fischer, G. (2010). High
 431 resolution profiles of vertical particulate organic matter export off Cape
 432 Blanc, Mauritania: Degradation processes and ballasting effects. *Deep*
 433 *Sea Research Part I: Oceanographic Research Papers*, 57(6), 771–784. doi:
 434 10.1016/j.dsr.2010.03.007
- 435 Iversen, M. H., & Ploug, H. (2010). Ballast minerals and the sinking carbon flux in
 436 the ocean: carbon-specific respiration rates and sinking velocity of marine snow
 437 aggregates. *Biogeosciences*, 7(9), 2613–2624. doi: 10.5194/bg-7-2613-2010
- 438 Iversen, M. H., & Ploug, H. (2013). Temperature effects on carbon-specific respi-
 439 ration rate and sinking velocity of diatom aggregates—potential implications
 440 for deep ocean export processes. *Biogeosciences*, 10(6), 4073–4085. doi:
 441 10.5194/bg-10-4073-2013
- 442 Iversen, M. H., & Robert, M. L. (2015). Ballasting effects of smectite on aggregate
 443 formation and export from a natural plankton community. *Marine Chemistry*,
 444 175, 18–27. doi: 10.1016/j.marchem.2015.04.009
- 445 Jackson, G. A. (1998). Using fractal scaling and two-dimensional particle size spec-
 446 tra to calculate coagulation rates for heterogeneous systems. *Journal of Colloid*
 447 *and Interface Science*, 202(1), 20–29. doi: 10.1006/jcis.1998.5435
- 448 Jackson, G. A. (2015). Coagulation in a rotating cylinder. *Limnology and Oceanog-*
 449 *raphy: Methods*, 13(4), 194–201.
- 450 Jackson, G. A., & Burd, A. B. (1998). Aggregation in the marine environ-
 451 ment. *Environmental Science & Technology*, 32(19), 2805–2814. doi:
 452 10.1021/es980251w
- 453 Jokulsdottir, T., & Archer, D. (2016). A stochastic, Lagrangian model of sinking
 454 biogenic aggregates in the ocean (SLAMS 1.0): model formulation, valida-
 455 tion and sensitivity. *Geoscientific Model Development*, 9(4), 1455–1476. doi:
 456 10.5194/gmd-9-1455-2016
- 457 Jouandet, M.-P., Trull, T. W., Guidi, L., Picheral, M., Ebersbach, F., Stem-
 458 mann, L., & Blain, S. (2011). Optical imaging of mesopelagic particles
 459 indicates deep carbon flux beneath a natural iron-fertilized bloom in the
 460 Southern Ocean. *Limnology and Oceanography*, 56(3), 1130–1140. doi:
 461 10.4319/lo.2011.56.3.1130
- 462 Kajihara, M. (1971). Settling velocity and porosity of large suspended particle.
 463 *Journal of the Oceanographical Society of Japan*, 27(4), 158–162. doi: 10.1007/
 464 bf02109135
- 465 Kiørboe, T. (2001). Formation and fate of marine snow: small-scale processes with

- 466 large-scale implications. *Sci Mar*, *65*, 57–71.
- 467 Kwon, E. Y., Primeau, F., & Sarmiento, J. L. (2009). The impact of remineraliza-
468 tion depth on the air–sea carbon balance. *Nature Geoscience*, *2*(9), 630–635.
469 doi: 10.1038/ngeo612
- 470 Laurenceau-Cornec, E. C., Trull, T. W., Davies, D. M., De La Rocha, C. L., &
471 Blain, S. (2015). Phytoplankton morphology controls on marine snow sinking
472 velocity. *Marine Ecology Progress Series*, *520*(Buesseler 1998), 35–56. doi:
473 10.3354/meps11116
- 474 Laurenceau-Cornec, E. C., Le Moigne, F. A., Gallinari, M., Moriceau, B., Toullec,
475 J., Iversen, M. H., . . . De La Rocha, C. L. (2020). New guidelines for the
476 application of Stokes’ models to the sinking velocity of marine aggregates.
477 *Limnology and Oceanography*, *65*(6), 1264–1285. doi: 10.1002/lno.11388
- 478 Lin, M., Lindsay, H., Weitz, D., Ball, R., Klein, R., & Meakin, P. (1989).
479 Universality in colloid aggregation. *Nature*, *339*(6223), 360–362. doi:
480 10.1038/339360a0
- 481 Logan, B. E., & Wilkinson, D. B. (1990). Fractal geometry of marine snow and
482 other biological aggregates. *Limnology and Oceanography*, *35*(1), 130–136. doi:
483 10.4319/lno.1990.35.1.0130
- 484 Loth, E. (2008). Drag of non-spherical solid particles of regular and irregular shape.
485 *Powder Technology*, *182*(3), 342–353. doi: 10.1016/j.powtec.2007.06.001
- 486 Marsay, C. M., Sanders, R. J., Henson, S. A., Pabortsava, K., Achterberg, E. P.,
487 & Lampitt, R. S. (2015). Attenuation of sinking particulate organic carbon
488 flux through the mesopelagic ocean. *Proceedings of the National Academy of
489 Sciences*, *112*(4), 1089–1094. doi: 10.1073/pnas.1415311112
- 490 McDonnell, A. M., & Buesseler, K. O. (2010). Variability in the average sinking ve-
491 locity of marine particles. *Limnology and Oceanography*, *55*(5), 2085–2096. doi:
492 10.4319/lno.2010.55.5.2085
- 493 Meakin, P. (1987). Fractal aggregates. *Advances in Colloid and Interface Science*,
494 *28*, 249–331. doi: 10.1016/0001-8686(87)80016-7
- 495 Miklasz, K. A., & Denny, M. W. (2010). Diatom sinkings speeds: Improved pre-
496 dictions and insight from a modified Stokes’ law. *Limnology and Oceanography*,
497 *55*(6), 2513–2525.
- 498 Mouw, C. B., Barnett, A., McKinley, G. A., Gloege, L., & Pilcher, D. (2016). Phyto-
499 plankton size impact on export flux in the global ocean. *Global Biogeochemical
500 Cycles*, *30*(10), 1542–1562. doi: 10.1002/2015gb005355
- 501 Nowald, N., Fischer, G., Ratmeyer, V., Iversen, M., Reuter, C., & Wefer, G. (2009).
502 In-situ sinking speed measurements of marine snow aggregates acquired with
503 a settling chamber mounted to the Cherokee ROV. In (pp. 1–6). IEEE. doi:
504 10.1109/oceanse.2009.5278186
- 505 Oseen, C. W. (1910). Über die Stokes’ sche Formel und Über eine verwandte Auf-
506 gabe in der Hydrodynamik. *Arkiv Mat., Astron. Och Fysik*, *6*, 1.
- 507 Reynolds, R. A., & Stramski, D. (2021). Variability in oceanic particle size dis-
508 tributions and estimation of size class contributions using a non-parametric
509 approach. *Journal of Geophysical Research: Oceans*, *126*(12), e2021JC017946.
- 510 Serra-Pompei, C., Soudijn, F., Visser, A. W., Kiørboe, T., & Andersen, K. H.
511 (2020). A general size-and trait-based model of plankton communities.
512 *Progress in Oceanography*, *189*, 102473. doi: 10.1016/j.pocean.2020.102473
- 513 Serra-Pompei, C., Ward, B. A., Pinti, J., Visser, A. W., Kiørboe, T., & Ander-
514 sen, K. H. (2022). Linking plankton size spectra and community com-
515 position to carbon export and its efficiency. *Global Biogeochemical Cycles*,
516 e2021GB007275.
- 517 Smoluchowski, M. v. (1916). Drei vortrage über diffusion, brownische bewegung und
518 koagulation von kolloidteilchen. *Zeitschrift für Physik*, *17*, 557–585.
- 519 Stemmann, L., Eloire, D., Sciandra, A., Jackson, G., Guidi, L., Picheral, M., &
520 Gorsky, G. (2008). Volume distribution for particles between 3.5 to 2000 μm

- 521 in the upper 200 m region of the South Pacific Gyre. *Biogeosciences*, 5(2),
522 299–310.
- 523 Stokes, G. G. (1851). On the effect of the internal friction of fluids on the motion of
524 pendulums. *Transactions of the Cambridge Philosophical Society*, 9(8).
- 525 Suess, E. (1980). Particulate organic carbon flux in the oceans—surface productivity
526 and oxygen utilization. *Nature*, 288(5788), 260–263. doi: 10.1038/288260a0
- 527 Syvitski, J. P., Asprey, K., & Leblanc, K. (1995). In-situ characteristics of particles
528 settling within a deep-water estuary. *Deep Sea Research Part Ii: Topical Stud-*
529 *ies in Oceanography*, 42(1), 223–256. doi: 10.1016/0967-0645(95)00013-g
- 530 Tappan, H., & Loeblich Jr, A. R. (1973). Evolution of the oceanic plankton. *Earth-*
531 *Science Reviews*, 9(3), 207–240. (Publisher: Elsevier)
- 532 Toktamış, D., Toktamış, H., & Yazıcı, A. N. (2016). The effects of thermal treat-
533 ments on the thermoluminescence properties of biogenic minerals present in
534 the seashells. *Radiation Effects and Defects in Solids*, 171(11-12), 951–964.
- 535 Tréguer, P., & Jacques, G. (1992). Review Dynamics of nutrients and phytoplank-
536 ton, and fluxes of carbon, nitrogen and silicon in the Antarctic Ocean. In *Wed-*
537 *dell Sea Ecology* (pp. 149–162). Springer. doi: 10.1007/978-3-642-77595-6_17
- 538 Van der Jagt, H., Friese, C., Stuut, J. W., Fischer, G., & Iversen, M. H. (2018).
539 The ballasting effect of Saharan dust deposition on aggregate dynamics and
540 carbon export: Aggregation, settling, and scavenging potential of marine snow.
541 *Limnology and Oceanography*, 63(3), 1386–1394. doi: 10.1002/lno.10779
- 542 Visser, A. W., & Jónasdóttir, S. H. (1999). Lipids, buoyancy and the seasonal verti-
543 cal migration of *Calanus finmarchicus*. *Fisheries Oceanography*, 8, 100–106.
- 544 White, F. M. (1991). *Viscous Fluid Flow*. New York, NY: McGraw-Hill.
- 545 Wiesner, M. R. (1992). Kinetics of aggregate formation in rapid mix. *Water Re-*
546 *search*, 26(3), 379–387. doi: 10.1016/0043-1354(92)90035-3

Table 1. Estimated exponent $b \pm s$ for excess density vrs aggregate size power law where s is the 95% confidence interval. Δ_r is the $\log_{10} r$ range of aggregate size, and n the number of observations. References as given, and indicate field or lab studies.

b	$\pm s$	Δ_r	n		<i>reference</i>	
-0.38	1.21	0.5	14		(Alldredge & Gotschalk, 1989)	Field
-1.49	0.15	1.9	76		(Alldredge & Gotschalk, 1988)	Field
-2.09	1.22	0.5	13	i	(Azetsu-Scott & Johnson, 1992)	Field
-1.09	1.88	0.4	15	ii	---	Lab
-0.72	0.20	0.8	37		(Iversen et al., 2010)	Field
-0.83	0.55	0.9	104		(Belcher et al., 2016)	Field
-1.11	0.94	0.8	10		(Carder et al., 1982)	Field
-2.18	0.28	1.0	332		(Diercks & Asper, 1997)	Field
-1.07	0.09	1.2	294		(Engel & Schartau, 1999)	Lab
-1.21	0.05	1.1	20		(Gibbs, 1985)	Field
-1.46	0.05	1.6	1224		Chase 1979	Field
-1.13	0.14	1.1	63	i	(Iversen & Ploug, 2010)	Lab
-1.20	0.12	0.8	26	ii	---	Lab
-1.01	0.20	0.5	97	iii	---	Lab
-0.46	0.30	0.5	99		(Hill et al., 1998)	Field
-0.51	0.23	0.9	187		(Iversen & Ploug, 2013)	Lab
-1.34	0.26	1.1	153		(Iversen & Robert, 2015)	Lab
-1.37	0.20	1.4	54		(Kajihara, 1971)	Field
-2.12	0.59	0.8	61	i	(Laurenceau-Cornec et al., 2015)	Field
-1.24	0.21	0.8	59	ii	---	Lab
-1.24	0.21	0.8	72	i	(Laurenceau-Cornec et al., 2020)	Lab
-0.35	0.19	0.7	131	ii	---	Lab
-1.53	0.12	1.2	274	i	(Engel et al., 2009)	Lab
-1.07	0.09	1.2	249	ii	---	Lab
-0.74	0.14	1.2	296	iii	---	Field
-1.53	0.70	0.9	49		(Nowald et al., 2009)	Field
-1.22	0.12	1.7	149		(Syvitski et al., 1995)	Field
-0.95	0.37	1.3	57	i	(Van der Jagt et al., 2018)	Field
-2.01	0.30	1.2	85	ii	---	Field
-0.88	0.23	1.9	36		(Guidi et al., 2008)	Field
-1.65	0.26	1.7	41		(McDonnell & Buesseler, 2010)	Field
-2.24	0.78	1.0	28		(Jouandet et al., 2011)	Field
-1.59	0.02	1.2	1654		(Bach et al., 2019)	Field
-0.11	0.25	0.7	36		(Gärdes et al., 2011)	Lab
-1.74	0.27	1.4	154		(Iversen & Lampitt, 2020)	Field
-1.38	0.02	4.0	6332		All data points	-